An *LC* Decoupling Network for Two Antennas Working at Low Frequencies

Huan Meng and Ke-Li Wu, *Fellow, IEEE*

***Abstract*— This paper presents an *LC* low-pass π network to decouple a pair of coupled antennas working at low frequencies. Comparing with existing decoupling techniques, the proposed decoupling network provides a wideband but compact decoupling solution. Moreover, a generalized one-fit-all scheme is justified to implement the decoupling network with an antenna independent core network. By adjusting a few external components, the same core network can be applied to a collection of antenna pairs with different coupling levels and antenna form factors. Four design examples are given to demonstrate the unique features of the proposed network for low-frequency applications. In all cases, the decoupling network significantly improves the isolation between two antennas over a wide frequency band while the intrinsic matching bandwidth of the antennas is maintained.**

***Index Terms*— Decoupling network, multiple input multiple output (MIMO) antenna array, mutual coupling, network synthesis.**

I. Introduction

THE multiple-input multiple-output (MIMO) technology using multiple antennas has been proven to be an effective data access scheme for improving the data throughput in a multipath rich environment by incorporating with advanced signal processing techniques such as spatial multiplexing or diversity coding, that the MIMO technology is able to increase the data throughput by a great amount [1], [2]. The technology has been successfully used in commercial operations of the fourth-generation mobile networks. Nowadays, MIMO technique has been widely used in Long-Term Evolution (LTE) wireless system, utilizing not only high-frequency bands in gigahertz range but also low-frequency bands in a range of hundreds of megahertz. However, the benefits brought by the multiple antenna technique will be significantly degraded by the inevitable mutual couplings among antennas in practice. It is particularly true in low-frequency bands for a mobile phone as the electrical spacing between antennas is very small. The mutual coupling reduces the radiation efficiency of each antenna, the signal-to-noise ratio caused by the interference between antennas, and eventually, the data throughput. In low-frequency band cases, in which the separation between antennas is much smaller than half a wavelength, the signal spatial correlation among each antenna increases drastically, which introduces further degradation of data throughput [3].

A great amount of work has been devoted to developing effective and practical decoupling techniques to reduce the mutual couplings among antennas. Existing decoupling mechanisms in general fall into three categories. The first category is based on mode decompositions [4], [5]. By introducing a hybrid coupler, it is possible to excite a pair of antennas with two orthogonal modes that decorrelate the signal from the antennas. In theory the approach is applicable to an MIMO system consists of arbitrary number of antennas but a bulky coupler network is always required. The second category of decoupling techniques employs artificial structures such as electromagnetic bandgap or defected ground structure for altering the current distribution on the ground. The artificial structure introduces a current redistribution, which changes the radiation pattern and possibly decreases the mutual coupling [6], [7]. Compared with the mode-based approaches, the artificial structure technique offers a wider bandwidth. However, the approach is an *ad hoc* solution and its real estate usually is in a large fraction of wavelength. Since the design heavily depends on the antenna geometries, a small change in antenna design may require a complete redesign of the structure and therefore limited applications can be found. The third type of decoupling techniques applies a shunt connected passive network to cancel the mutual admittance between two coupled antennas. The network is carefully designed to introduce an opposite admittance to cancel the mutual admittance of the antenna pair and thereby improves the isolation. The passive network may have different implementations, such as a neutralization line [8] or dummy elements terminated with a reactive load [9]. However, the former significantly reduces the matching bandwidth while the latter requires an additional space to host dummy elements. References [10] and [11] employ the same idea with a lumped implementation of the decoupling network for WiFi applications. However, both designs are not suitable for antennas working at low frequencies because the lumped component values become extremely large at the working frequencies.

Recently, a coupled-resonator decoupling network (CRDN) technique is proposed to improve the isolation between two antenna ports [12]. The network is connected in parallel

Manuscript received July 23, 2016; revised November 3, 2016; accepted January 16, 2017. Date of publication February 14, 2017; date of current version June 29, 2017. This work was supported in part by the Research Grants Council of the Hong Kong Special Administrative Region, China, under Project CUHK 410713, and in part by the Development and Reform Commission of Shenzhen Municipality under Grant Shen Fa Gai (2013) 1673. This paper is an expanded version from the 2015 Asia–Pacific Microwave Conference, Nanjing, China, December 6–9, 2015. *(Corresponding author: Ke-Li Wu.)*

The authors are with the Department of Electronic Engineering, The Chinese University of Hong Kong, Shatin, Hong Kong (e-mail: hmeng@ee.cuhk.edu.hk; klwu@ee.cuhk.edu.hk).

Color versions of one or more of the figures in this paper are available online at http://ieeexplore.ieee.org.

Digital Object Identifier 10.1109/TMTT.2017.2658562

with the antenna pairs to cancel their mutual admittance. Comparing with other antenna decoupling approaches, the CRDN technique provides a wideband solution for decoupling with a good bandpass frequency selectivity. Moreover, the CRDN can be directly designed once the S-parameters of the coupled antennas are known with a deterministic design procedure. An LTCC version of a CRDN module with a one-fit-all decoupling solution is proposed in [13]. By changing the input–output (I/O) coupling, the same decoupling module can accommodate different coupled antenna form factors with different coupling levels.

In a recent conference paper, a decoupling network that employs an *LC* low-pass π network is proposed by Meng and Wu [14]. As compared to the CRDN decoupling technique, it has been found out that the *LC* π network has following two distinct advantages: 1) it offers a much wider decoupling bandwidth and 2) it provides a compact decoupling solution for antennas working in low-frequency range owing to its nonresonance property. The second feature is particularly important for low-frequency MIMO applications such as LTE bands within the 700 MHz range. However, no theoretic proof is provided to explain the bandwidth improvement. Besides, the design of the *LC* π network is highly dependent on the antennas parameters. No discussion is given on the theory of a one-fit-all solution of this *LC* decoupling network.

In this paper, two important aspects concerned to this *LC* decoupling network are addressed: 1) a rigorous mathematical proof is provided to explain the two distinct advantages and 2) a one-fit-all solution of this *LC* decoupling approach is proposed and theoretically studied, which lays the foundation for developing an integrated decoupling passive chip. With the proposed one-fit-all solution, an integrated passive decoupling module can be developed to accommodate various pair of coupled antennas not only with different coupling levels but also with different antenna form factors. It will only require to redesign a few external components to simultaneously satisfy the decoupling and matching conditions as long as the original coupled antennas are well matched. The generalized one-fit-all *LC* decoupling network provides an effective low-frequency decoupling solution.

This paper is organized as follows. The detailed theoretical framework is provided in Section II, including a review of the design theory for the shunt connected decoupling network, a theoretic bandwidth analysis and a derivation of the one-fit-all design. Four design examples are then provided in Section III to demonstrate the effectiveness of the presented approach and the one-fit-all feature by experimental results. Finally, a conclusion is given in Section IV to summarize the work.

II. Design Theory

A. General Design Equations

Considering the system described by the block diagram shown in Fig. 1 and denoting the admittance matrix of the coupled antenna pair with their ports extended by a matched transmission line θ_1 as $\mathbf{Y_A}$, and the admittance matrix of an *LC* decoupling π network shown in Fig. 2 as $\mathbf{Y_N}$, the overall admittance matrix equals to the summation of $\mathbf{Y_A}$ and $\mathbf{Y_N}$ as

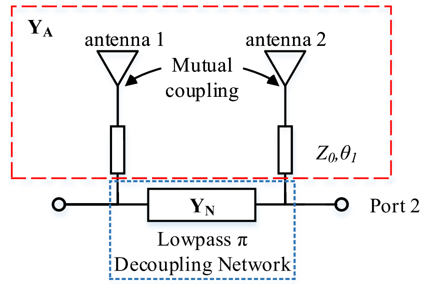

Fig. 1. Network representation of a coupled-antenna pair in parallel with an *LC* π decoupling network.

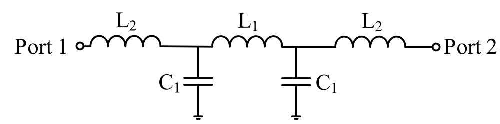

Fig. 2. *LC* π decoupling network.

they are connected in parallel

$$\mathbf{Y} = \begin{bmatrix} Y_{11} & Y_{12} \\ Y_{21} & Y_{22} \end{bmatrix} = \begin{bmatrix} Y_{11}^A + Y_{11}^N & Y_{12}^A + Y_{12}^N \\ Y_{21}^A + Y_{21}^N & Y_{22}^A + Y_{22}^N \end{bmatrix}. \tag{1}$$

A good isolation between two antenna ports requires that

$$Y_{21}(\omega_0) = Y_{12}^A(\omega_0) + Y_{12}^N(\omega_0) \approx 0. \tag{2}$$

Here ω_0 denotes the working frequency for decoupling. Assuming the decoupling network is lossless, its admittance matrix is purely imaginary. On the other hand, the admittance parameter of a coupled antenna pair in general is complex in values. To satisfy the decoupling condition (2), a piece of matched transmission line are needed at each antenna port to enforce Y_{12}^A being purely imaginary at the working frequency. The electrical length θ_1 is determined by the phase of S_{21}, φ_{21}, of the coupled antenna pair as

$$\theta_1 = \frac{1}{2}\left[\varphi_{21} \pm k\pi - \frac{\pi}{2}\right], \quad k = 0, 1, 2, 3.... \tag{3}$$

Furthermore, it is assumed that the coupled antennas are well matched so the imaginary part of its self-admittance Y_{11}^A and Y_{22}^A tends to be very small. In this case, the self-admittance of the decoupling network is required to satisfy the following condition to maintain the same matching:

$$\operatorname{Im}\{Y_{ii}^N(\omega_0)\} \approx 0, \quad i = 1, 2. \tag{4}$$

In summary, knowing the admittance parameters $\mathbf{Y_A}$, the electrical length θ_1 is first determined by (3) to guarantee a good isolation to be admissible. After adding θ_1 at each port, the decoupling network is designed by enforcing the decoupling condition (2) and the matching condition (4) to its admittance parameters. To this end, either a direct synthesis approach or a generic circuit optimizer may be applied.

B. Bandwidth Analysis

A theoretical proof is provided in this section to justify the wide band feature of the decoupling network. The proof compares the slope of admittance parameters versus frequency for an *LC* π-network with that of the CRDN. It will be demonstrated that the proposed decoupling network always preserves a wider decoupling bandwidths. Because a CRDN in nature is a bandpass network, the filter theory can be applied to analyze its frequency behavior. By the classical filter design theory, a prototype network refers to a template circuit based on which a physical filter can be built with a proper frequency transformation.

Assume an *LC* decoupling network and a CRDN are designed based on the same prototype network. Denote the angular frequency variable in the prototype domain as Ω, and the physical frequencies for the *LC* π-network and the CRDN as ω_L and ω_B, respectively. The prototypes for *LC* low-pass and bandpass frequency transformations are, respectively, given by

$$\Omega = \frac{1}{\omega_{Lc}}\omega_L \tag{5a}$$

$$\Omega = \frac{\omega_{B0}}{\Delta\omega_B}\left(\frac{\omega_B}{\omega_{B0}} - \frac{\omega_{B0}}{\omega_B}\right) \tag{5b}$$

where ω_{Lc} refers to the cutoff frequency of a proposed π network, ω_{B0} and $\Delta\omega_B$ denote the center frequency and the bandwidth of a CRDN, respectively.

In fact, (2) and (4) only stipulate perfect isolation and matching conditions at ω_0. Apparently, the decoupling bandwidth depends on the slope for the mutual admittance versus frequency. If the admittance has a small slope over the frequency range of interest, a wider decoupling bandwidth can be obtained. However, the matching bandwidth depends on the Q factor of the antennas and matching network. The slope for mutual admittances of the proposed network and a CRDN can be found, respectively, as

$$\frac{dy_{21}}{d\omega_L} = \frac{dy_{21}}{d\Omega}\cdot\frac{d\Omega}{d\omega_L} = \frac{dy_{21}}{d\Omega}\cdot\frac{1}{\omega_{Lc}} \tag{6a}$$

$$\frac{dy_{21}}{d\omega_B} = \frac{dy_{21}}{d\Omega}\cdot\frac{d\Omega}{d\omega_B} = \frac{dy_{21}}{d\Omega}\cdot\frac{\omega_B^2+\omega_{B0}^2}{\Delta\omega_B\cdot\omega_B^2} \approx \frac{dy_{21}}{d\Omega}\cdot\frac{2}{\Delta\omega_B} \tag{6b}$$

with y_{21} being the mutual admittance parameters of the prototype filter. The approximation in (6b) is valid for ω_B in the vicinity of the center frequency ω_{B0}.

A comparison of (6a) and (6b) reveals that the slope of y_{21} for the proposed network is inversely proportional to the cutoff frequency ω_{Lc} of the *LC* low-pass π network whereas the slope of a CRDN is inversely proportional to its bandwidth $\Delta\omega_B$. In practice, the CRDN bandwidth $\Delta\omega_B$ is limited to a fraction of ω_{B0} but the cutoff frequency ω_{Lc} of an *LC* low-pass π network is in the same order of ω_{B0}. Therefore, the mutual admittance of the π-network changes versus frequency with a much smaller rate. It is worth to mention that for an even order design, the term $dy_{21}/d\Omega$ on the right-hand side of (6a) and (6b) may be slightly different for the two different types of decoupling networks. This is because for an even order CRDN, the working frequency usually is defined by ω_{B0}, corresponding to $\Omega = 0$, where the slope of y_{21} is flat at zeros of y_{11} and y_{22}. However, for the *LC* low-pass π-network, it is impossible to set its working frequency corresponding to $\Omega = 0$. In practice, the working frequency of the proposed decoupling network is designed at a frequency corresponding to the second zero of the y_{11} and y_{22}, where $\Omega \neq 0$ in the prototype domain. An illustration is given in Fig. 3(a), showing the admittance parameters of a sixth-order prototype filter. If the same prototype is used for decoupling, the working frequency of a CRDN will be set at ω_{B0}, which is equivalent to $\Omega = 0$ shown by the hollow circles in the porotype domain. For the proposed π-network, the working frequency should be designed at a value that corresponds to the second zero of y_{11} above $\Omega = 0$, as indicated by the solid circles. For an odd degree design, the term $dy_{21}/d\Omega$ in (6a) and (6b) have identical values as y_{11} and y_{22} do not pass zero at $\Omega = 0$. The admittance parameters of a fifth-order prototype network are shown in Fig. 3(b) for illustration. In that case, both the proposed network and the CRDN will set the working frequency corresponding to the same admittance zero indicated by the hollow squares in Fig. 3(b). The slope is then solely determined by the cutoff frequency or the bandwidth. Nevertheless, for both cases, the slope is mainly determined by ω_{Lc} and $\Delta\omega_B$ rather than $dy_{21}/d\Omega$. Therefore, the proposed network always has a much smaller slope or wider decoupling bandwidth than that of a CRDN. Last but not least, in general the lower the filter order, the smaller $dy_{21}/d\Omega$ will be observed. Therefore in practice a low order network is always preferred when designing the decoupling network.

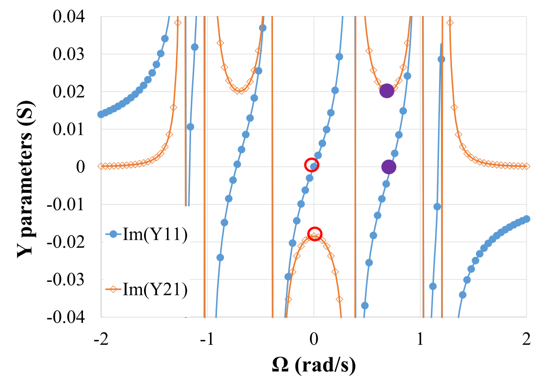

(a)

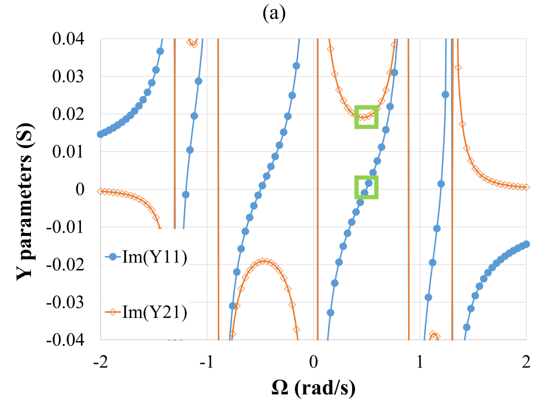

(b)

Fig. 3. Admittance parameters of (a) even order prototype network and (b) odd order prototype network.

C. One-Fit-All Scheme

The idea of developing a one-fit-all decoupling module is first proposed in [13] for a CRDN, with which the same integrated passive module can be utilized to decouple antenna

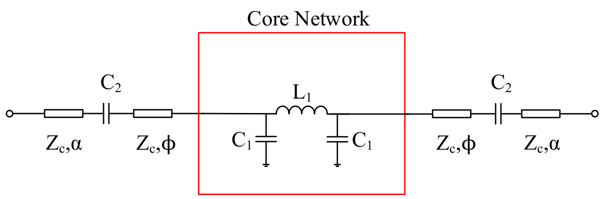

Fig. 4. Proposed one-fit-all decoupling network with an integrated LC π-network module.

pairs with different coupling level and different antenna form factors. It is found that the concept is also applicable to the proposed LC decoupling network. Without loss of generality, the design in this paper is only confined to symmetric networks, but it is also applicable to asymmetric networks. Fig. 4 shows a third-order one-fit-all LC decoupling π network for illustrations. The inductor L_1 in the original circuit shown in Fig. 2 is replaced with two sections of transmission lines with a capacitor C_2 connected in between while the core network remains unchanged. Denote the characteristic impedance of both transmission lines as Z_c and the electrical lengths as α and ϕ, respectively. The input admittances of the half network with the symmetry plane being short or open is given by

$$y_{\text{in}}^{\text{odd}} = \frac{Z_c + \tan\alpha \left\{\frac{1}{\omega C_2} + \frac{jZ_c[jZ_c \tan\phi + 1/\Delta]}{[Z_c + j\tan\phi/\Delta]}\right\}}{Z_c\left\{jZ_c\tan\alpha - j/(\omega C_2) + \frac{Z_c[jZ_c\tan\phi + 1/\Delta]}{[Z_c + j\tan\phi/\Delta]}\right\}} \tag{7a}$$

$$y_{\text{in}}^{\text{even}} = \frac{Z_c + \tan\alpha \left\{\frac{1}{\omega C_2} + \frac{j\,Z_c[j\,Z_c\tan\phi - j/(\omega C_1)]}{[Z_c + \tan\phi/(\omega C_1)]}\right\}}{Z_c\left\{j\,Z_c\tan\alpha - j/(\omega C_2) + \frac{Z_c[j\,Z_c\tan\phi - j/(\omega C_1)]}{[Z_c + \tan\phi/(\omega C_1)]}\right\}} \tag{7b}$$

where $\Delta = j\omega C_1\text{-}2j/(\omega L_1)$.

The admittance parameters of the decoupling network are related to the even/odd mode input admittance through

$$Y_{11}^N = \frac{1}{2}\left(y_{\text{in}}^{\text{even}} + y_{\text{in}}^{\text{odd}}\right) \quad \text{and} \quad Y_{21}^N = \frac{1}{2}\left(y_{\text{in}}^{\text{even}} - y_{\text{in}}^{\text{odd}}\right). \tag{8}$$

After substitution of (7) into (8), it is apparent that both Y_{11}^N and Y_{21}^N are functions of C_2 and ϕ. Here, α is selected as a design parameter. Therefore, it is possible to design a circuit with adjustable Y_{21}^N while Y_{11}^N being enforced to 0 at the working frequency by changing the capacitor C_2 and the electrical length ϕ only. Fig. 5 shows the loci for different values of Y_{21}^N as a function of C_2 and ϕ for illustration. Besides, the locus of Y_{11}^N that satisfies the matching condition is also superposed in the figure. The intersect of the Y_{11}^N curve with any Y_{21}^N curve represents a possible solution for simultaneously decoupling and matching for a prescribed Y_{21}^N. This example is designed at 700 MHz with other circuit components as $C_1 = 1$ pF, $L_1 = 15$ nH, $Z_c = 100\ \Omega$ and α is set to be 60°. It is shown that with a set of feasible values of C_2 and ϕ, the condition $Y_{11}^N = 0$ can be satisfied for different prescribed Y_{21}^N values.

To validate the solutions in Fig. 5, the corresponding decoupling networks are simulated with the same component values as those in Fig. 5. The simulated Y_{21}^N is shown in Fig. 6,

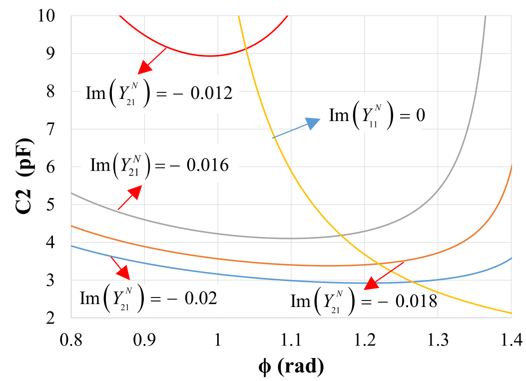

Fig. 5. Loci of the $\text{Im}(Y_{11}^N) = 0$ and $\text{Im}(Y_{21}^N) = -0.2$ to -0.016 for $C_1 = 1$ pF, $L_1 = 15$ nH, $Z_c = 100\ \Omega$, and $\alpha = 60°$ designed at 700 MHz.

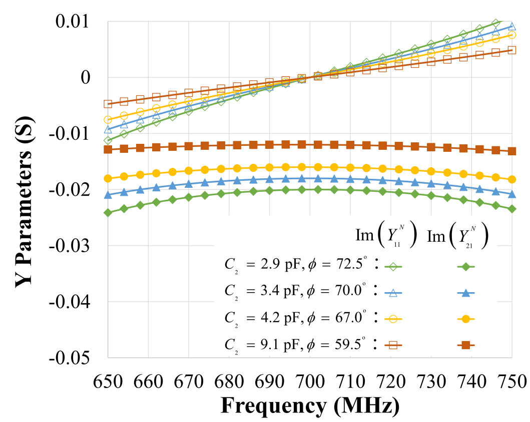

Fig. 6. Simulated admittance parameters of the decoupling network for different C_2 and ϕ for achieving negative Y_{21}^N.

showing the condition of $Y_{11}^N = 0$ being well satisfied at the working frequency 700 MHz for all cases. It is interesting to note that for all four solutions, the value of ϕ only slightly changes. In practice this small change can be realized by adjusting the soldering pad size. Therefore, in practice only C_2 needs to be changed to accommodate different coupling levels.

In addition to being able to accommodate different negative Y_{21}^N values, the same one-fit-all module can also realize different positive Y_{21}^N values. To this end, the electrical length α should be adjusted in addition to changing C_2 and ϕ. This generalized one-fit-all feature is very attractive for practical applications as it suggests an antenna independent core network for decoupling different antenna problems as long as their working frequency is the same. Once the internal core network has been developed, the same module can be applied to a collection of antenna pairs by adjusting only a few external components regardless of antenna forms.

III. Design Examples

Four design examples are given in this section. The first example implements a fifth-order decoupling π-network in an LTCC surface mountable device for decoupling an inverted-F antenna (IFA) pair working at 1.27 GHz. The objective is to demonstrate the proposed compact decoupling solution for

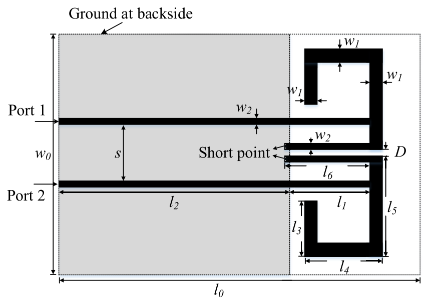

Fig. 7. PCB layout of two coupled IFA antennas working at 1.27 GHz.

TABLE I
DIMENSIONS OF THE IFA ANTENNA PAIR IN FIG. 7 (mm)

w_0	52		l_0	100		l_4	19.7
w_1	3		l_1	21.2		l_5	23
w_2	1.52		l_2	6.45		l_6	23.2
D	0.16		l_3	11		s	15.1

a low-frequency application. The other three examples use lumped *LC* components to prove the concept of one-fit-all decoupling scheme. A pair of monopole antennas working at 740 MHz is used in the second, third, and fourth examples. The coupling between the last two pairs of antennas is intentionally designed with a different strength. Electromagnetic (EM) simulations are done by HFSS.

A. LTCC Decoupling Device for a 1.27 GHz IFA Pair

A pair of IFA antennas working at 1.27 GHz is prototyped on an FR4 PCB substrate for demonstration purpose. The antenna layout is shown in Fig. 7, and all dimensions are listed in Table I. The FR4 substrate is with a relative dielectric constant of 4.4 and a thickness of 0.8 mm. The EM simulated S-parameters are shown in Fig. 10(a). It is seen the coupling between the two antennas is around -6 dB at the working frequency. According to (3), the value of $\theta_1$is first determined to be $-55°$ at 1.27 GHz. After the phase at each antenna port being shifted by θ_1, Y_{21}^A becomes $-0.021j$. Due to the limited space between two antennas and the semilumped nature of an LTCC device, the decoupling network is designed with the *LC* π-network shown in Fig. 2. In order to simultaneously satisfy both decoupling and matching conditions, the required component values in the circuit model are $L_1 = 3.57$ nH, $C_1 = 1.51$ pF, and $L_2 = 2.18$ nH. For comparison, to decouple the same antenna pair with a CRDN, the total required inductance and the capacitance are, respectively, 42.7 nH and 3.1 pF, which are determined by following the procedures in [13]. Definitely, it is very challenging to come by with a 42 nH inductor inside a compact device while the proposed *LC* decoupling π-network is more realistic in size and therefore more attractive for low-frequency MIMO systems. Based on the obtained *LC* π circuit model, an LTCC device is then developed and prototyped. The 3-D layout of the LTCC device is shown in Fig. 8(a), and the fabricated LTCC device is shown in Fig. 8(b). The LTCC device is with a compact dimension of $2 \times 1.25 \times 0.95$ mm^3. Fig. 9 shows a photograph of the coupled IFA antennas with the LTCC decoupling device surface mounted in shunt with the antennas at the location that is shifted by $\theta_1$from each antenna port. The measured S-parameters of the decoupled antennas are superposed with those of the coupled antennas as shown in Fig. 10(a). It can be observed that the isolation is significantly improved from 6 to 23 dB at 1.27 GHz and the 10 dB isolation bandwidth is approximately 90 MHz, or equivalently a 7% fractional bandwidth, whereas the matching bandwidth remains almost unaffected.

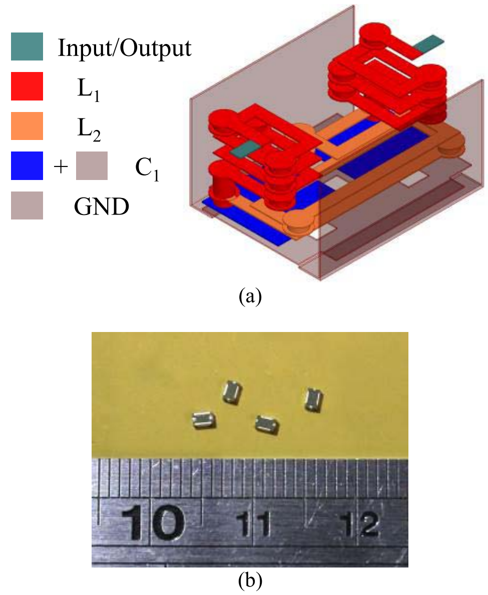

Fig. 8. (a) EM model. (b) Fabricated LTCC decoupling device.

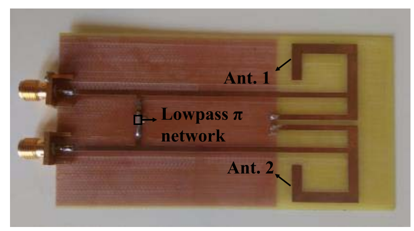

Fig. 9. Fabricated IFA antenna pair with the LTCC decoupling device.

Moreover, the radiation efficiency is also investigated. Ideally, the amount of increased radiation power is equal to that of the coupled power being reduced if the decoupling network is lossless and the matching remains unchanged. Thus it is estimated from Fig. 10(a) that the improvement in efficiency will be 24%. The measured radiation efficiency is shown in Fig. 10(b). As can be seen, the radiation efficiency at 1.27 GHz is increased from 55% to 70%, which is consistent with the estimation if the loss of the network is taken into account. The efficiency enhancement further provides a proof of the proposed decoupling scheme.

B. Pair of Weakly Coupled Monopole Antennas

To verify the one-fit-all concept, a pair of monopole antennas working at 740 MHz are designed and prototyped on an FR4 substrate with a relative dielectric constant of 4.4 and a

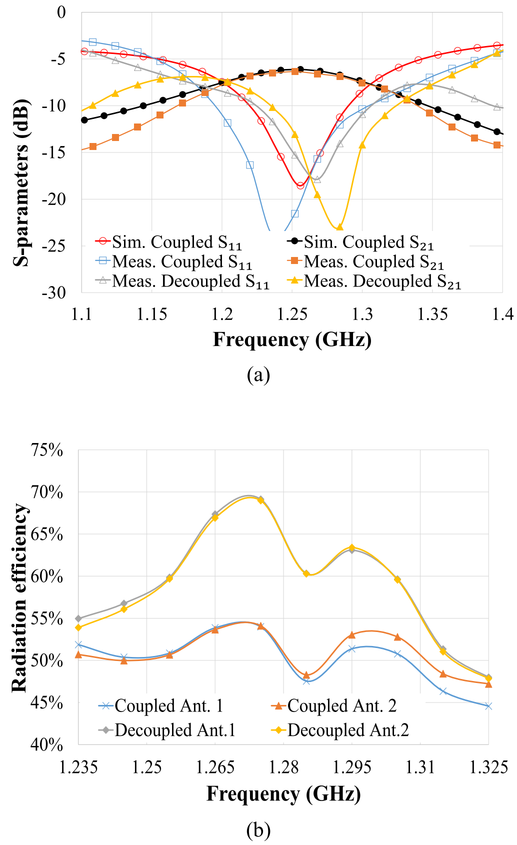

Fig. 10. Measured performance of the prototype antenna pairs working at 1.27 GHz with and without the LTCC decoupling device. (a) S-parameters. (b) Antenna radiation efficiency.

thickness of 1.6 mm. In this example, the separation between the monopole antennas is deliberately set to be 0.16 λ_0 to introduce a relatively weak coupling, where λ_0 refers to the free space wavelength at 740 MHz. The layout of the antenna pair with interconnection lines α and ϕ for the decoupling network is shown in Fig. 11. All dimensions are listed in Table II. The gap g_1 is designed for mounting the lumped capacitor C_2 and the inductor L_1, while g_2 is designed for mounting the shunt capacitor C_1. Based on the EM simulation of the coupled monopole antennas, the components of the *LC* π decoupling network are determined by following a similar procedure as that in the first example. However, the one-fit-all decoupling network shown in Fig. 4 is adopted this time to verify the concept. To satisfy the decoupling condition, the required mutual admittance *YN 21* at the working frequency is $-0.0152j$ after the antenna port is properly shifted by $\theta_1 = -9.4°$. The optimized decoupling network are $\alpha = 45°$, $C_2 = 15$ pF, $\phi = 25°$, $C_1 = 5.7$ pF, and $L_1 = 14.3$ nH. Here all electrical lengths are referenced at 740 MHz. These electrical lengths, including θ_1, α, and ϕ, are then converted to physical lengths. To account for the discontinuities of the bend, the dimensions l_3 to l_6 are slightly adjusted, and the final dimensions are listed in Table II. In this example, surface mount inductors and capacitors are used to implement the decoupling network. Fig. 12 shows the simulated and the measured responses for both coupled and decoupled cases. Due to the manufacture

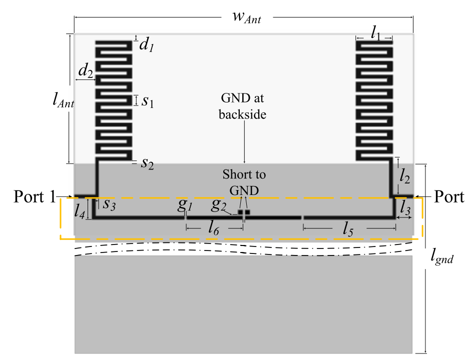

Fig. 11. Two weakly coupled monopole antennas working at 740 MHz and the layout of decoupling circuit without *LC* components mounted.

TABLE II

DIMENSIONS OF THE WEAKLY COUPLED ANTENNA PAIR IN FIG. 11 (mm)

l_{Ant}	38	l_1	10.5	l_5	26.4	s_2	1
w_{Ant}	97	l_2	11	l_6	16	s_3	1
d_1	2	l_3	5	l_{gnd}	102	g_1	0.7
d_2	6	l_4	6.16	s_1	3	g_2	0.35

TABLE III

DIMENSIONS OF THE STRONGLY COUPLED ANTENNA PAIR IN FIG. 14 (mm)

w_{Ant}	80	l_6	3	l_{10}	3.8
l_1	11	l_7	6.1	l_{gnd}	82
l_3	2	l_8	3.2		
l_5	24	l_9	22.6		

error, the measurement result of the coupled response slightly deviates from the simulation result in Fig. 12(a), which leads to an inaccurate design of the decoupling network. As shown in Fig. 12(b), the 10 dB matching bandwidth is a little bit narrower compared to the simulated ones. Nevertheless, the measured isolation is improved from 8 to 20 dB at the working frequency. In addition, the envelope correlation coefficient (ECC) calculated from the measured radiation patterns is plotted in Fig. 13, showing a significant reduction after inserting the decoupling network. Moreover, the radiation efficiency is also improved from 65% to 72% at the designed frequency. In this example, the efficiency enhancement is limited by the loss of the surface mountable *LC*. An integrated passive decoupling device may provide a better efficiency improvement if efficiency is of the primary concern.

C. Pair of Strongly Coupled Monopole Antennas

This example adopts the core circuit designed for the second example. The same pair of monopole antennas are used but the separation distance is reduced to 0.11 λ_0. The layout of the coupled antennas is shown in Fig. 14. Table III summarizes the dimensions that are either with different values or not used in the layout in Fig. 11. The ground size is also deliberately reduced to increase the coupling. As shown in Fig. 15, the simulated EM response of the coupled antennas has a strong coupling of -6 dB at 740 MHz. Based on the EM simulation, the electrical length θ_1 that enforces Y_{21}^A being purely imaginary is first determined to be $-13.65°$. For a good isolation, $Y_{21}^N = -0.022j$ is required. Keeping L_1, C_1,

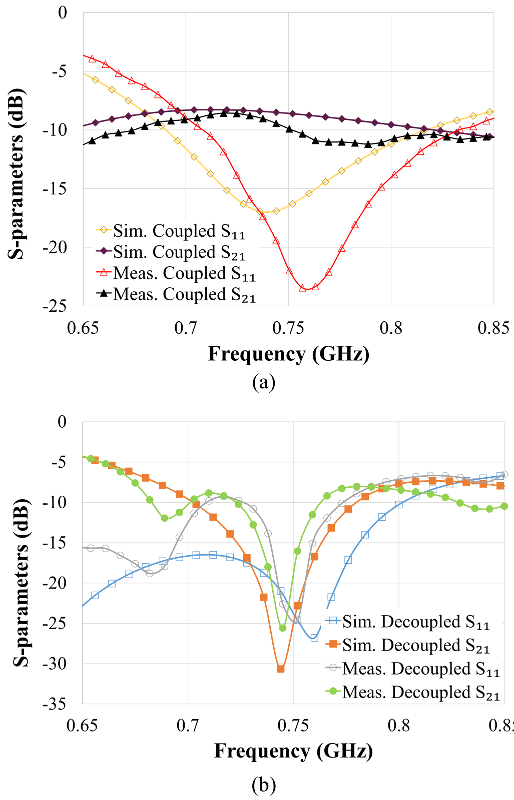

Fig. 12. Simulated and measured scattering parameters of the weakly coupled monopole antenna pair. (a) Coupled antennas. (b) Decoupled antennas.

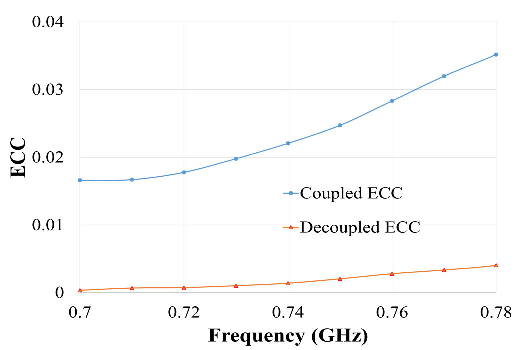

Fig. 13. ECC of the weakly coupled monopole pair.

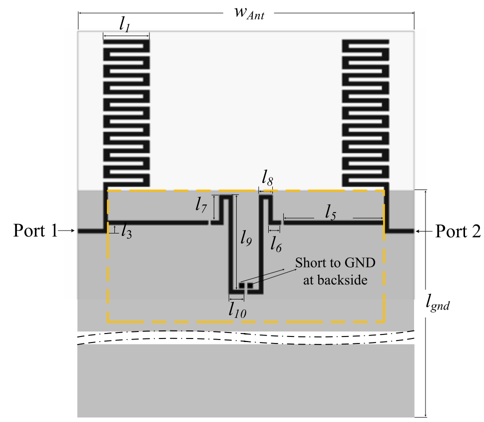

Fig. 14. Two strongly coupled monopole antennas working at 740 MHz and layout of decoupling circuit without *LC* components mounted.

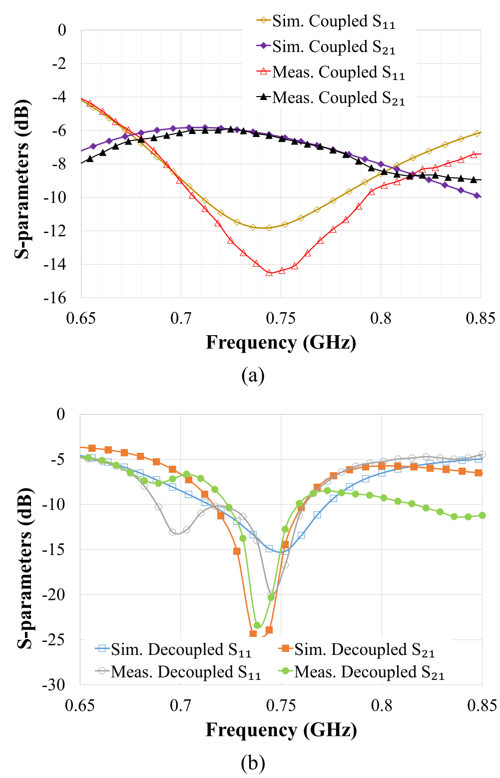

Fig. 15. Simulated and measured scattering responses of the strongly coupled monopole pair. (a) Coupled response. (b) Decoupled response.

and α unchanged, the values of ϕ and C_2 that satisfy both the decoupling and matching conditions can be numerically determined by solving (8). The obtained values for ϕ and C_2 are 37.9° and 4.31 pF, respectively.

Fig. 15 shows the simulated and measured responses for both the coupled and decoupled monopole pairs. It can be seen that the isolation is improved from 6 to 25 dB at the working frequency while the matching after decoupling antennas is comparable to that of the coupled case. The measured radiation patterns of the coupled array and the decoupled array are shown in Fig. 16. The ECC is calculated and is plotted in Fig. 17. It is proved that the insertion of the decoupling network not only improves the isolation but also reduces the ECC of the two antennas. Moreover, the radiation efficiency at 740 MHz is also increased from 58% to 67%.

D. Pair of Extremely Strongly Coupled Monopole Antennas

The same core circuit as in previous two examples is used in this example concerning two extremely strong coupled monopole antenna pair with center frequency of 740 MHz to demonstrate the capability of decoupling of two extremely strong coupled wideband antennas. The coupled antenna pair is the same as that in the third example except the ground dimension l_{gnd} is now reduced to 32 mm, resulting a poor isolation of 2.15 dB. In addition, as shown in Fig. 19, the bandwidth of 10 dB matching of the coupled antennas is 200 MHz. Following the proposed procedure, it is found that when $\theta_1 = 2.5°$, Y_{21}^A becomes purely imaginary with a value of $0.023j$. Keeping L_1, C_1, and α same as those in

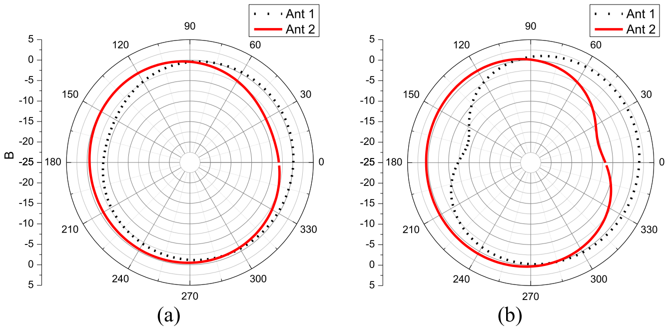

Fig. 16. Measured radiation patterns at 740 MHz in xoy plane of (a) coupled array and (b) decoupled array.

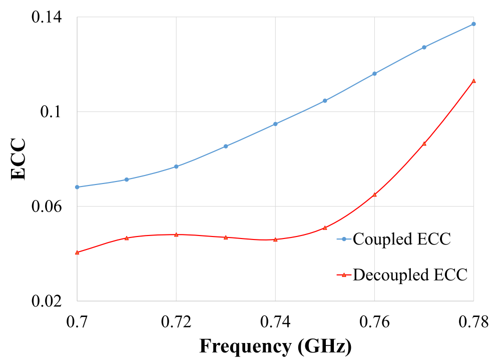

Fig. 17. ECC of the strongly coupled monopole pair.

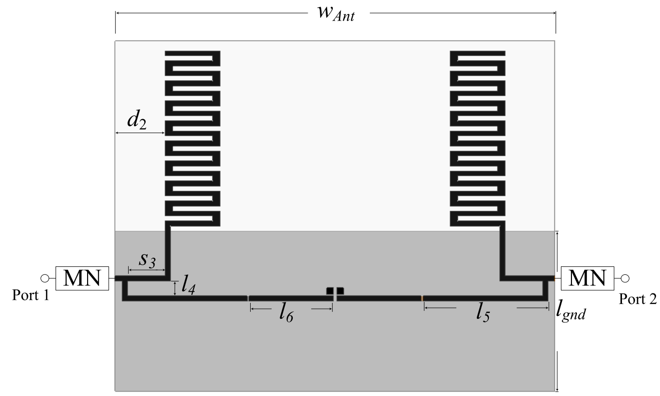

Fig. 18. Two extremely strong coupled monopole antennas working at 740 MHz and the layout of decoupling circuit without *LC* components. A matching network is inserted at each port.

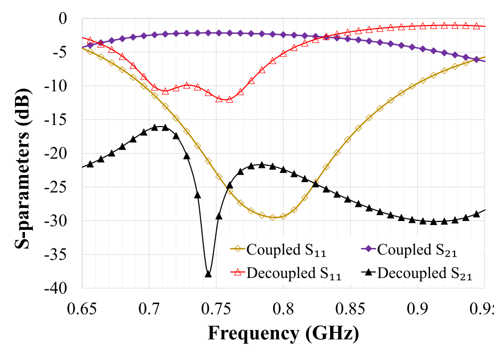

Fig. 19. Simulated scattering responses of the extremely strong coupled monopole pair.

previous two examples, the values of ϕ and C_2 are found to be 25.16° and 5.2 pF, respectively. The layout of the coupled array with the required decoupling transmission lines but without the *LC* circuit is shown in Fig. 18. The dimensions shown in the figure are: $w_{\mathrm{Ant}} = 88$, $d_2 = 10$, $s_3 = 8.6$, $l_4 = 3$, $l_5 = 25$, $l_6 = 17$, and $l_{\mathrm{gnd}} = 32$ (units: mm). All other dimensions are the same as those in the third example. The EM model shown in Fig. 18 is then cosimulated with the required discrete *LC* components. In this extremely strong coupled example, the wide band impedance matching is a fake matching because the coupled antenna acts as a matched resistive load due to the strong mutual coupling. Once the mutual coupling is significantly reduced, the matching condition is expected to be deteriorated seriously. Therefore, a matching network is needed at each antenna port. The simulated scattering parameters of the decoupled antennas with a matching network at each antenna port are superposed in Fig. 19. It can be observed that the decoupling bandwidth of more than 15 dB isolation is 300 MHz, or more than 40% decoupling bandwidth, whereas the matching bandwidth of -10 dB is more than 80 MHz or more than 10%, which is a very wide impedance matching bandwidth for such an electrical small antenna array. It must be point out that the decoupling circuit could not improve the intrinsic impedance bandwidth of an antenna.

Through the four examples, it has been demonstrated that the proposed one-fit-all scheme can provide a compact decoupling solution for the antennas working at low frequencies down to a few hundreds of megahertz.

IV. Conclusion

An *LC* π-network is proposed for decoupling two coupled antennas working at low frequencies in this paper. With the decoupling and matching conditions satisfied simultaneously, the proposed decoupling network can be realized in a one-fit-all scheme, which allows the core circuit of the network to be integrated into one consolidated device for different antenna coupling levels. A theoretic proof shows that the proposed decoupling network provides a wider decoupling bandwidth as compared with other decoupling techniques. The most distinct feature of the proposed decoupling network is that it is highly suitable for antennas working at low frequencies because of its simple circuit topology and small required *LC* components. Four design examples working at low frequencies are provided to validate the concept, including an LTCC integrated decoupling device, two examples using the lumped element circuit version of the proposed decoupling network, and an example involving two extremely strong coupled monopole antennas. The experimental results for three cases and one EM simulated case have demonstrated that the proposed decoupling network is simple to implement and effective for a wide range of coupled antenna problems working in low-frequency bands.

References

[1] R. Vaughan and J. B. Anderson, *Channels, Propagation and Antennas for Mobile Communications*. London, U.K.: IEE, 2003.

[2] M. A. Jensen and J. W. Wallace, "A review of antennas and propagation for MIMO wireless communications," *IEEE Trans. Antennas Propag.*, vol. 52, no. 11, pp. 2810–2824, Nov. 2004.

[3] J. B. Andersen, "Array gain and capacity for known random channels with multiple element arrays at both ends," *IEEE J. Sel. Areas Commun.*, vol. 18, no. 11, pp. 2172–2178, Nov. 2000.

[4] L. K. Yeung and Y. E. Wang, "Mode-based beamforming arrays for miniaturized platforms," *IEEE Trans. Microw. Theory Techn.*, vol. 57, no. 1, pp. 45–52, Jan. 2009.

[5] C. Volmer, J. Weber, R. Stephan, K. Blau, and M. A. Hein, "An eigen-analysis of compact antenna arrays and its application to port decoupling," *IEEE Trans. Antennas Propag.*, vol. 56, no. 2, pp. 360–370, Feb. 2008.

[6] F. Yang and Y. Rahmat-Samii, "Microstrip antennas integrated with electromagnetic band-gap (EBG) structures: A low mutual coupling design for array applications," *IEEE Trans. Antennas Propag.*, vol. 51, no. 10, pp. 2936–2946, Oct. 2003.

[7] L. Yang, M. Fan, F. Chen, J. She, and Z. Feng, "A novel compact electromagnetic-bandgap (EBG) structure and its applications for microwave circuits," *IEEE Trans. Microw. Theory Techn.*, vol. 53, no. 1, pp. 183–190, Jan. 2005.

[8] A. Diallo, C. Luxey, P. Le Thuc, R. Staraj, and G. Kossiavas, "Enhanced two-antenna structures for universal mobile telecommunications system diversity terminals," *IET Microw. Antennas Propag.*, vol. 2, no. 1, pp. 93–101, Feb. 2008.

[9] L. Zhao and K.-L. Wu, "A decoupling technique for four-element symmetric arrays with reactively loaded dummy elements," *IEEE Trans. Antennas Propag.*, vol. 62, no. 8, pp. 4416–4421, Aug. 2014.

[10] S. C. Chen, Y. S. Wang, and S. J. Chung, "A decoupling technique for increasing the port isolation between two strongly coupled antennas," *IEEE Trans. Antennas Propag.*, vol. 56, no. 12, pp. 3650–3658, Dec. 2008.

[11] C.-H. Wu, C.-L. Chiu, and T.-G. Ma, "Very compact fully lumped decoupling network for a coupled two-element array," *IEEE Antennas Wireless Propagat. Lett*, vol. 15, pp. 158–161, 2016.

[12] L. Zhao, L. K. Yeung, and K.-L. Wu, "A coupled resonator decoupling network for two-element compact antenna arrays in mobile terminals," *IEEE Trans. Antennas Propag.*, vol. 62, no. 5, pp. 2767–2776, May 2014.

[13] K. Qian, L. Zhao, and K.-L. Wu, "An LTCC coupled resonator decoupling network for two antennas," *IEEE Trans. Microw. Theory Techn.*, vol. 63, no. 10, pp. 3199–3207, Oct. 2015.

[14] H. Meng and K.-L. Wu, "A lowpass decoupling network for two coupled antennas," in *Proc. Asia–Pacific Microw. Conf.*, Dec. 2015, pp. 1–3.

Huan Meng received the B.Eng. degree (with first-class Hons.) in electronic and information engineering from The Hong Kong Polytechnic University, Hong Kong, in 2010, and the M.Phil. degree in electronic engineering from The Chinese University of Hong Kong, Hong Kong, in 2012, where he is currently pursuing the Ph.D. degree.

His current research interests include the synthesis, design, and computer aided tuning of passive microwave coupled-resonator networks, including diplexers and multiplexers.

Ke-Li Wu (M'90–SM'96–F'11) received the B.S. and M.Eng. degrees from the Nanjing University of Science and Technology, Nanjing, China, in 1982 and 1985, respectively, and the Ph.D. degree from Laval University, Québec, QC, Canada, in 1989.

From 1989 to 1993, he was with the Communications Research Laboratory, McMaster University, Hamilton, ON, Canada, as a Research Engineer and a Group Manager. In 1993, he joined the Corporate Research and Development Division, COM DEV International, Cambridge, ON, the largest Canadian space equipment manufacturer, where he was a Principal Member of Technical Staff. Since 1999, he has been with The Chinese University of Hong Kong, Hong Kong, where he is a Professor and the Director of the Radiofrequency Radiation Research Laboratory. He has authored numerous publications in the areas of EM modeling and microwave passive components, microwave filter, and antenna engineering. His current research interests include partial element equivalent circuit and physically derived micromodeling circuits for high-speed circuits, RF and microwave passive circuits and systems, synthesis theory and robot automatic tuning of microwave filters, decoupling techniques for multiple antennas in both wireless terminals, and massive multi-in multi-out array antennas.

Prof. Wu is a member of the IEEE MTT-8 Subcommittee (Filters and Passive Components) and also serves as a TPC member for many prestigious international conferences including the IEEE MTT-S International Microwave Symposium. He was the recipient of the 1998 COM DEV Achievement Award for the development of exact EM design software of microwave filters and multiplexers and the Asia–Pacific Microwave Conference Prize in 2008 and 2012, respectively. He was an Associate Editor of the IEEE TRANSACTIONS ON MICROWAVE THEORY AND TECHNIQUES from 2006 to 2009.